Boundary-Layer Meteorology (2021) 180:407–433
https://doi.org/10.1007/s10546-021-00637-x

RESEARCH ARTICLE

Intermittent Surface Renewals and Methane Hotspots in Natural Peatlands

Enrico Zorzetto[1] · Olli Peltola[2] · Tiia Grönholm[3] · Gabriel G. Katul[4,5]

Received: 14 December 2020 / Accepted: 9 June 2021 / Published online: 4 July 2021

Abstract
Peatlands account for a large fraction of global methane (CH_4) emissions. These environments exchange CH_4 with the atmosphere via three main mechanisms: diffusion through the peat and water, plant-mediated diffusion, and sporadic release of CH_4 bubbles. While rapid advances have been made in measuring CH_4 fluxes above peatlands on sub-daily time scales, partitioning CH_4 fluxes into ebullition and background diffusion remains a formidable challenge. Such partitioning is becoming necessary for future projection of methane concentration as atmospheric, hydrologic, and edaphic drivers of these two types of methane releases may differ significantly. Using surface renewal theory, a framework for partitioning measured methane fluxes based on the mass transfer mechanism is introduced with the overall objective of characterizing the intermittency of CH_4 source and its strength at the ground. This approach is tested using a large dataset of measured turbulent air velocity and multiple scalar concentrations (including heat, water vapour, and carbon dioxide) for flow above a boreal peatland in Finland. The transport efficiencies of different gas transfer mechanisms are then evaluated for scalars characterized by background diffusion (e.g., water vapour) or by intermittent sources (e.g., methane). Whether environmental variables such as water-table levels and atmospheric conditions have a signature on the occurrence of CH_4 hotspots is then investigated. Building upon the classical surface renewal theory, this work introduces a novel approach for inferring the intermittent nature of scalar sources at the ground and for exploring how non-homogeneity affects the efficiency of gas turbulent transport in the atmospheric surface layer.

Keywords Atmospheric surface layer · Methane ebullition · Surface renewal theory · Wavelet decomposition · Intermittent gas exchange

✉ Enrico Zorzetto
ez6263@princeton.edu

1 Program in Atmospheric and Oceanic Sciences, Princeton University, Princeton, NJ, USA

2 Climate Research Programme, Finnish Meteorological Institute, Helsinki, Finland

3 Atmospheric Composition Research, Finnish Meteorological Institute, Helsinki, Finland

4 Nicholas School of the Environment, Duke University, Durham, NC, USA

5 Department of Civil and Environmental Engineering, Duke University, Durham, NC, USA

1 Introduction

Methane (CH_4) fluxes are emitted in many types of natural and managed ecosystems including wetlands, peatlands, and rice fields (Bartlett and Harriss 1993; Aulakh 2001), but their magnitude is highly variable (Byrne et al. 2004; Lai 2009; Hommeltenberg et al. 2014; Knox et al. 2019). CH_4 fluxes are conventionally measured using gas chambers positioned at the ground surface (Bubier et al. 1993; Moore et al. 2011; Beetz et al. 2013) or by means of micrometeorological methods such as the eddy-covariance technique (Rinne et al. 2007; Herbst et al. 2011; Baldocchi et al. 2012; Hommeltenberg et al. 2014). The release of methane from the ground occurs via three main mechanisms: molecular diffusion through the saturated soil surface, diffusion through the aerenchymatous tissue in plants (Riutta et al. 2020), and release of methane through bubbles (ebullition). The latter is by far the more variable mechanism, as the gas bubbles are emitted sporadically and can lead to significant mass transfer rates that are localized in time and in space.

Because of the co-occurrence of these different sources at the ground, the overall CH_4 fluxes in these environments can exhibit a marked variability in space and time. This peculiarity can produce significant difficulties in measuring CH_4 exchange with conventional gas chambers covering a small fraction of the ground area. Rapid advancements in gas analyzers have been made over the past two decades, allowing for direct measurements of methane turbulent fluxes above the ground using the eddy-covariance technique. These measurements are able to resolve methane fluxes on a sub-hourly time scale over a sufficiently large 'footprint', but on the other hand do not distinguish between ebullition, plant-mediated, and background emissions. The spatially intermittent source characterizing CH_4 fluxes has been observed to lead to scalar concentration fluctuations that are much more 'heavy-tailed' than their carbon dioxide (CO_2), water vapour (H_2O), or air temperature counterparts, even above ecosystems that appear to be reasonably uniform (Peltola et al. 2013; Katul et al. 2018b). These differences in concentration statistics provide information relevant for partitioning measured CH_4 fluxes into a background and an intermittent (hotspot) contribution, the goal here.

A partition methodology based on the wavelet transform was recently proposed (Iwata et al. 2018) to partition CH_4 fluxes based on the scalar similarity with a reference scalar (water vapour). Here, a similar technique is employed to characterize the fraction of flux, scalar variance, and footprint area that carry the signature of localized CH_4 hotspots. Then, based on these quantities, the surface renewal theory (Higbie 1935; Danckwerts 1951) is extended to characterize mass exchange for scalars such as CH_4 that are characterized by an intermittent source at the ground. The surface renewal theory has a long history in atmospheric sciences and has been applied to turbulent transfer of heat and water vapour (Brutsaert 1965, 1975; Clayson et al. 1996; Haghighi and Or 2013, 2015b, a; Katul and Liu 2017) assuming that Kolmogorov size eddies dominate interfacial transport. However, prior models based on continuous renewal of the surface are not directly applicable to characterizing CH_4 emissions originating from intermittent sources at the ground. In fact, as early as 1961, it was already acknowledged that the presence of zero-contact times (no renewal) has a significant effect on estimated fluxes, effect which can be larger than that of the specific probability distribution used to model contact times (Perlmutter 1961).

It is precisely this intuition that is to be exploited here to model CH_4 interfacial mass transfer. That is, parcels of air may be continually refreshed via ejections and sweeps, but the absence of the 'hotspot' source may be viewed as a no-renewal time when compared to other scalars such as H_2O or CO_2. To be clear, the surface renewal method developed here must be regarded as a pragmatic approach to partitioning measured CH_4 fluxes into

their background component and the contribution from spatially intermittent hotspots. We expect these hotspots to be statistically related to the occurrence of ebullition events, or potentially to spatial variability in the distribution of plants and microbial activity. These hypotheses are examined by relating the partitioned CH_4 fluxes to environmental variables previously documented as controlling gas exchange (e.g., seasonality, atmospheric pressure, and water-table-level changes). With imminent proliferation of methane eddy-covariance flux measurements worldwide, the proposed surface renewal scheme can be complementary to other measurement approaches and modelling efforts aimed at quantifying the magnitude and intermittency of CH_4 fluxes across various ecosystems and environmental conditions.

The manuscript is organized as follows: in Sect. 2, key definitions and a brief review of turbulent scalar exchange in the atmospheric surface layer are provided with a focus on the conventional surface renewal theory and its limitations in describing fluxes of scalar quantities characterized by intermittent and sparse sources or sinks at the ground. Section 3 describes the experimental set-up and data used. Section 4 describes the partition scheme based on the wavelet decomposition, which is employed for partitioning scalar fluxes and scalar variances into contributions connected to background or hotspot fluxes respectively. This partitioning assumes that ground sources of water vapour are reasonably uniform and not contaminated by hotspots. Thus, water vapour offers a 'satellite' scalar for the quantification of background statistics. Based on this partition, Sect. 5 introduces the surface renewal scheme used to model scalar fluxes for the set-up here. The classic surface renewal is extended to describe scalars such as CH_4 that are characterized by spatially and temporally inhomogeneous fluxes. In Sect. 6, implications of the results are discussed with a focus on the frequency and the transport efficiency of the methane hotspot fluxes, as well as an investigation of their potential dependence on the aforementioned slowly evolving environmental variables.

2 Turbulent Mass Transfer and Surface Renewal Theory

The transport of momentum, heat, and other scalar quantities in the lower atmosphere is primarily driven by turbulent eddies generated by the interplay between shear and buoyancy forces (Wyngaard 2010; Stull 2012), traditionally described by Monin–Obukhov similarity theory (MOST) (Monin and Obukhov 1954; Foken 2006). For stationary and planar-homogeneous flow at high Reynolds numbers in the absence of mean subsidence and mean pressure gradients, the mean momentum and continuity equations for any scalar c reduce to

$$\frac{d\overline{u'w'}}{dz} = 0; \frac{d\overline{w'c'}}{dz} = 0, \tag{1}$$

with u and w the velocity components in the direction of the mean wind x and in the vertical direction z, respectively. Here the overline represents averaging over coordinates of statistical homogeneity (time in this case) and s' denotes the instantaneous fluctuation from the mean of a generic variable s, so that $\overline{s'} = 0$. Therefore, $\overline{u'w'}$ is the net downward flux of momentum to the ground, $\overline{w'c'}$ the turbulent flux of any scalar with positive values signifying emissions and negative values signifying uptake, and c is the scalar concentration representing either CH_4, H_2O, CO_2, or temperature T. Integrating Eq. 1 with respect to z leads to the so-called constant-flux assumption, meaning that turbulent fluxes measured at some reference height z_r above a surface represent the emissions or uptake at the surface (Foken and Nappo 2008; Li et al. 2018).

In general, eddy-covariance measurements of methane assume that measured turbulent fluxes are constant with height but that MOST atmospheric stability corrections for methane differ from their water vapour or carbon dioxide counterparts due to dissimilarities in sources and sinks at the ground or entrainment from the free atmosphere. In the case of methane, the source strength at the ground is statistically patchy whereas for water vapour or carbon dioxide, the ground sources or sinks are comparatively uniform (or at least better blended). Hence, the effective eddy diffusivity from MOST may differ among scalars because the same air parcels making contact with the ground and subsequently ejecting continually exchanges water vapour and carbon dioxide with the surface, but less so for methane in the absence of ebullition. This assumption forms the basis of the extended surface renewal theory proposed here, where the presence of source hotspots is linked to a breakdown in the continuous surface renewal process.

Surface renewal theory has a long tradition in turbulence research and interfacial mass transfer. It was first introduced in the mid 1930s (Higbie 1935) and has been extensively applied to numerous interfacial mass and heat transfer problems (Danckwerts 1951; Hanratty 1956; Perlmutter 1961; Brutsaert 1965; Asher and Pankow 1991; Garbe et al. 2004). In its original form, mass exchange is driven by a surface concentration c_s and a background atmospheric concentration of the same substance c_a. The transport of any quantity c (e.g., mass, or possibly other quantities such as heat and momentum) is carried out by the arrival of elements of fresh fluid (i.e., turbulent eddies characterized by the background concentration c_a) to the surface, where the contact with the surface concentration c_s triggers unsteady molecular diffusion of the substance (or property) c. The conditions imposed on this transient diffusion are $c = c_a$ at $z > 0$, $t = 0$; $c = c_a$ for large z and $t > 0$; and $c = c_s$ at $z = 0$, $t > 0$. Solving this diffusion problem for a scalar with molecular diffusivity D_m yields the following expression for the instantaneous mass flux for a surface element characterized by age t (Danckwerts 1951; Brutsaert 1965; Horvath and Chatterjee 2018)

$$F(t) = D_m \left(\frac{\partial c}{\partial z} \right)_{z=0} = \Delta c \sqrt{\frac{D_m}{\pi t}}. \tag{2}$$

where $\Delta c = c_s - c_a$. After a certain residence time, each fluid element is ejected from the surface and immediately replaced by a fresh element with background concentration. This idealized model assumes that (i) only molecular diffusion into the air parcel in contact with the surface is allowed, (ii) the freshly renewed surface is characterized by a scalar concentration equal to the background concentration, and (iii) the time scales of sweep and ejection of the fluid parcel are small compared to the residence times of the parcel at the surface.

The distribution of contact times t on the surface depends on the characteristics of the flow. In the original Higbie model (Higbie 1935), each fluid parcel had the same residence time τ_c. The opposite situation is that studied by Danckwerts, in which the surface renewal is completely random (i.e., the renewal rate does not depend on eddy age). This assumption has been shown to lead to an exponential distribution of surface ages $p(\tau) = (1/b) \exp(-\tau/b)$, where $1/b$ is a surface renewal rate and $p(\tau)$ is the probability density function (p.d.f.) of τ (Danckwerts 1951). The following expression for the overall flux can now be derived based on an exponential $p(\tau)$

$$F_m = \int_0^\infty F(\tau) p(\tau) d\tau = \Delta c \int_0^\infty \sqrt{\frac{D_m}{\pi \tau}} \frac{1}{b} \exp\left(\frac{-\tau}{b} \right) d\tau = \Delta c \sqrt{\frac{D_m}{b}}. \tag{3}$$

Other functional forms have been considered for the distribution of surface ages $p(\tau)$, including gamma (Harriott 1962; Bullin and Dukler 1972) (that would arise in the case in

which younger surface eddies are less likely to be renewed when compared with the Danckwerts exponential distribution) and lognormal (Garbe et al. 2002), which is consistent with turbulence theories with internal intermittency in the turbulence kinetic energy dissipation rate accommodated. Several studies pointed out that the exact functional form of $p(\tau)$ is not important provided that its mean value is correct (Perlmutter 1961; Koppel et al. 1966; Seo and Lee 1988; Katul and Liu 2017) though others dispute this claim for water surfaces where local vertical advection can be large (Kermani and Shen 2009). To be clear, water surfaces do not admit a 'no-slip' condition, meaning that water velocity is finite (non-zero) at the air–water interface. This is not the case for the surfaces studied here, characterized by zero velocity at the interface.

In the micro surface renewal model used here, the residence times at the surface are of the order of the Kolmogorov time scale (Brutsaert 1965, 1975; Katul and Liu 2017; Katul et al. 2019). Surface renewal theory has also been applied to sensible heat flux assuming that large-scale coherent structures (often referred to as temperature ramps or ramp-cliff patterns (Antonia et al. 1979; Warhaft 2000; Zorzetto et al. 2018) dominate the scalar transfer (Qiu et al. 1995; Katul et al. 1996; Spano et al. 1997). A large-eddy model was also proposed to address the case of small Reynolds numbers, in which case scales much larger than the Kolmogorov microscale can be the primary contributors to the mass or heat transfer at the surface (Fortescue and Pearson 1967; Lamont and Scott 1970; Theofanous et al. 1976; Komori et al. 1990; Katul et al. 2018a).

Surface renewal theory has also been applied to the flux of momentum, with promising results reported from channel-flow experiments (Hanratty 1956; Thomson and Silver 1972; Musschenga et al. 1992). In the case of momentum, the role of the pressure term complicates the picture of the renewal processes when compared with passive scalar quantities, where molecular diffusion dominates the smallest scales of the flow. However, common to all these studies is the assumption that the renewal process at the surface is continuous. After presenting the experimental set-up (Sect. 3) and discussing the wavelet partitioning scheme (Sect. 4), in Sect. 5 this approach is generalized to the case of intermittent source at the ground, so as to tailor it to the case of CH_4 fluxes over peatlands.

3 Experiment

A published dataset (Katul et al. 2018b) collected at Siikaneva, a boreal wetland located in southern Finland, is analyzed. Briefly, velocity components and virtual temperature fluctuations were measured by an ultra-sonic anemometer. Two independent closed-path gas analyzers (LI-7000, LI-COR Biosciences, Lincoln, NE, USA; FMA, Los Gatos Research, USA) were used to measure H_2O, CO_2, and CH_4 concentrations, respectively. The analyzers sampled air just below the sonic anemometer (vertical separation 0.2 m) and shared a main inlet line. Measured concentrations for all gases were corrected to be relative to dry air.

All quantities were sampled at a frequency $f_s = 10$ Hz and stored in 30-min records with each 30-min record termed as a run. A total of 4416 runs were recorded between 1 June 2013 and 31 August 2013, of which 3743 passed standard quality checks with a length of at least 2^{14} sample points. Measurements were carried out at a height $z_r = 2.8$ m from the surface. We focus on data from a specific wind sector (from 230 to 270 degrees, i.e., primarily the south-west direction wind direction, conditions met by 643 runs out of 3743) to avoid wind sectors in which nearby forested areas could be part of the footprint and possibly contaminate the signal from the peatland. In the wind sector used here, the terrain

Fig. 1 Location of the experimental set-up site (Siikaneva I) in the Siikaneva fen in southern Finland. The image was obtained from the National Land Survey of Finland (2018)

is a reasonably homogeneous Boreal fen for several hundreds of metres. The locations of the tower and land cover are shown in Fig. 1.

For each run, the turbulent time series were despiked following the method proposed by Brock (1986), and recommended by Starkenburg et al. (2016). For CH_4, an additional check was performed: Any remaining fluctuations exceeding 60 standard deviations were removed and set equal to the median of the series. Coordinates were double-rotated such that $\overline{u}$ equals the average longitudinal velocity, with $\overline{v} = 0$ and $\overline{w} = 0$. A cross correlation analysis between w and scalar concentration was used to compute and correct the lag in the gas concentration time series. A stationarity check (Foken and Wichura 1996) was then applied to the fluxes of momentum $\overline{u'w'}$, temperature $\overline{w'T'}$, and water vapour $\overline{w'c'}$, with c' here denoting the fluctuations of the scalar H_2O. Some 2240 runs passed this test for all three quantities and with at least $N = 2^{14}$ data points.

The stationarity check was not applied to the CH_4 concentration time series since the objective is precisely the characterization of CH_4 fluxes possibly connected with short term localized emission events. Additionally, the runs in the dataset were filtered by requiring a minimum turbulence mixing ($u_* = \sqrt{-\overline{u'w'}} > 0.2\ \mathrm{m\,s^{-1}}$), a condition met by 1966 runs. We also required that the H_2O flux be upward ($\overline{w'c'}_{H_2O} > 0$) so as to avoid runs characterized by condensation, and that the H_2O turbulent concentration approximately follows the MOST variance–flux relation so as to avoid runs characterized by non-local effects and entrainment from the top of the atmospheric boundary layer as done in Iwata et al. (2018) and others for surface and roughness sublayer studies (Cava et al. 2008) or heat advection above lakes (Assouline et al. 2008). Out of 3743 runs, 1925 met this condition. These conditions of H_2O were prompted by the fact that water vapour is to be used as a reference scalar to partition the CH_4 signal based on the gas exchange mechanism, as discussed in Sect. 4. After applying these filters, a total of 274 30-min runs were included in the subsequent analyses.

4 Partitioning Methane Fluxes Using Concentration Measurements

Recent attention has been devoted to determining scalar fluxes originating from short turbulent events (Schaller et al. 2017) and to the partitioning of CH_4 fluxes connected with ebullition using wavelet transforms (Iwata et al. 2018; Schaller et al. 2019). Building upon these previous studies, the CH_4 time series is first analyzed in the wavelet domain with the objective of partitioning turbulent fluxes into their background (B) and hotspot (H) components. This partition will be used to calibrate the intermittent surface renewal (ISR) model when using another scalar to infer B. As recommended elsewhere (Iwata et al. 2018), we use water vapour as a reference scalar and explore scalar similarity in the Haar wavelet domain. Let c denote the concentration of the scalar of interest (e.g., methane here) and r the concentration of the reference scalar (H_2O). If scalar similarity holds (Hill 1989), then the two scalar time series should be perfectly correlated and the wavelet coefficients of the normalized time series $c_n = c'/\sigma_c$ and $r_n = r'/\sigma_r$ should also be equal (with $\sigma_c^2 = \overline{c'^2}$, $\sigma_r^2 = \overline{r'^2}$).

To localize CH_4 hotspot events both in the time and frequency domains, orthonormal wavelet transforms (Mallat 1989) are used. The scalar series are decomposed using the Haar wavelet basis, which has been widely applied to the study of turbulent flows (Meneveau 1991; Katul et al. 1994; Scanlon and Albertson 2001). The use of an orthonormal basis here is preferred because it does not introduce spurious information in the transformed series, and thus the scale-wise dependence between the two scalar time series is preserved by the transform (Katul et al. 1994; Kumar and Foufoula-Georgiou 1997). The Haar basis functions are of the form $\psi^{(m)}(x) = 2^{-m/2}\psi^{(0)}((x - 2^m i)/2^m)$ with $i, m \in Z$ the position and scale indices defining dilated and translated version of the Haar mother wavelet $\psi^{(0)}(x)$, defined as

$$\psi^{(0)}(x) = \begin{cases} 1 & \text{if } 0 < x < 1/2 \\ -1 & \text{if } 1/2 \leq x < 1. \\ 0 & \text{otherwise} \end{cases} \tag{4}$$

The wavelet coefficients $WT_f^{(m)}[i]$ can be computed by iteratively coarse-graining the generic series $f(t)$ as shown elsewhere (Katul et al. 1994)

$$WT_f^{(m)}[i] = \int_{-\infty}^{+\infty} f(t)\, \psi^{(m)}(t - i)\, dt. \tag{5}$$

In the wavelet domain, the flux of a scalar quantity c can be computed from its concentration measurement time series and vertical velocity as

$$\overline{F_c} = \overline{w'c'} = \frac{1}{N} \sum_{m=1}^{M} \sum_{i=1}^{2^{M-m}} WT_w^{(m)}[i] WT_c^{(m)}[i], \tag{6}$$

while the variance of the scalar can be obtained as

$$\sigma_c^2 = \overline{c'c'} = \frac{1}{N} \sum_{m=1}^{M} \sum_{i=1}^{2^{M-m}} \left(WT_c^{(m)}[i] \right)^2. \tag{7}$$

For each N observations per unit averaging interval ($N = 2^{14} = 16384$ data points per averaging period), the original series can be described from $N - 1$ wavelet coefficients $WT_f^m[i]$ (and the remaining coarse-grained series for wavelets with support longer than the Haar wavelet).

As also done by Iwata et al. (2018) to exploit the similarity between the scalar of interest and the reference scalar, both series are filtered thereby excluding from the analysis small scales within the inertial subrange and large scales for which (i) scalar similarity does not necessarily hold, and (ii) the poor time localization of the wavelet decomposition at the lowest frequencies may not provide sufficient information. Additionally, at small scales well within the inertial subrange, gas concentrations are characterized by the weakest signal-to-noise ratios (Peltola et al. 2014). Therefore, we focus our attention on the range of scales between $0.5\,T_w$ and $200\,T_w$, where T_w is the integral time scale of the vertical velocity fluctuation w'. For each run, T_w was computed by integrating the autocorrelation function of the w' series up to the first zero-crossing. This range of scales explains most of the variances and covariances for both CH_4 and H_2O. We define $\delta_s\,(m)$ as the indicator function selecting this range of scales (i.e., $\delta_s\,(m) = 1$ if $0.5 < 2^m/\,(f_s T_w) < 200$, and $\delta_s\,(m) = 0$ otherwise).

To quantify the distance between the coefficients $WT_c^{(m)}\,[i]$ and the corresponding reference scalar coefficients $WT_r^{(m)}\,[i]$, the slope and intercept of the linear relation $WT_c^{(m)}\,[i]\,/\sigma_c = \alpha_w WT_r^{(m)}\,[i]\,/\sigma_r + \beta_w$ are first determined. The α_w and β_w quantities are computed using a Huber regressor algorithm, which is particularly robust to the presence of outliers. The absolute differences $\Delta WT^{(m)}[i] = |WT_c^{(m)}[i]/\sigma_c - \alpha_w WT_r^{(m)}[i]/\sigma_r - \beta_w|$ between the wavelet coefficients of the two scalars $c(t)$ and $r(t)$ are then determined, and their standard deviation evaluated over the range of scales for which $\delta_s(m) = 1$

$$\Sigma_{cr} = \left(\overline{\left(\Delta WT^{(m)}[i] - \overline{\Delta WT^{(m)}[i]} \right)^2} \right)^{1/2}. \tag{8}$$

As expected, Σ_{cr} tends to decrease for increasing values of the correlation R_{cr} between the two scalars as shown in Fig. 2a for $c = CH_4$ and $r = H_2O$. In the case of perfect scalar similarity, the correlation between the two scalars should be $R_{cr} = 1$ and this difference should approach zero. Moreover, Fig. 2b shows that runs with larger Σ_{cr} are also characterized by CH_4 traces having a larger scalar skewness compared to their H_2O counterpart, as previously noted by Katul et al. (2018b). Here, the joint moments are defined as $M_{ij} = \overline{c^i w^j}/\sigma_c^i \sigma_w^j$ with σ_c, σ_w the root-mean-squared (r.m.s.) fluctuations of c and w, so that the skewness of the scalar c is M_{30}. In the presence of identical sources at the ground, this should not be the case, as noted by Hill (1989). This observation will be used to partition hotspot and background CH_4 coefficients.

For this purpose, we select a value of Σ_{cr} that is representative of the variability between the two time series that one would experience in the absence of differences in the sources or sinks at the ground. In the dataset here, this limiting standard deviation value is taken to be $\hat{\Sigma}_{rc} = 0.3$. As shown in Fig. 2, this threshold corresponds to runs characterized by R_{cr} closest to unity with CH_4 and H_2O exhibiting a comparable skewness. As done in Iwata et al. (2018), a threshold of $3\hat{\Sigma}_{rc}$ was adopted to determine whether or not any given CH_4 wavelet coefficient $WT_c^{(m)}[i]$ carries signature of localized hotspots. This partition was applied with this hard threshold to all the runs. For each run, the subset of the scale-time wavelet domain characterized by values of $\Delta WT^{(m)}[i] < 3\hat{\Sigma}_{cr}$ is characterized by a homogeneous ground source for the two scalar. Conversely, the condition for detecting hotspots is given by $\Delta WT^{(m)}[i] > 3\hat{\Sigma}_{rc}$. To perform this partitioniong, we denote with $\delta_x(i,m)$ the indicator function that selects hotspot events only ($x = h$: $\delta_h(i,m) = 1$ when $\Delta WT^{(m)}[i] > 3\hat{\Sigma}_{rc}$, else $\delta_h(i,m) = 0$) or background events only ($x = b$: $\delta_b(i,m) = 0$ when $\Delta WT^{(m)}[i] > 3\hat{\Sigma}_{rc}$, else $\delta_b(i,m) = 1$)

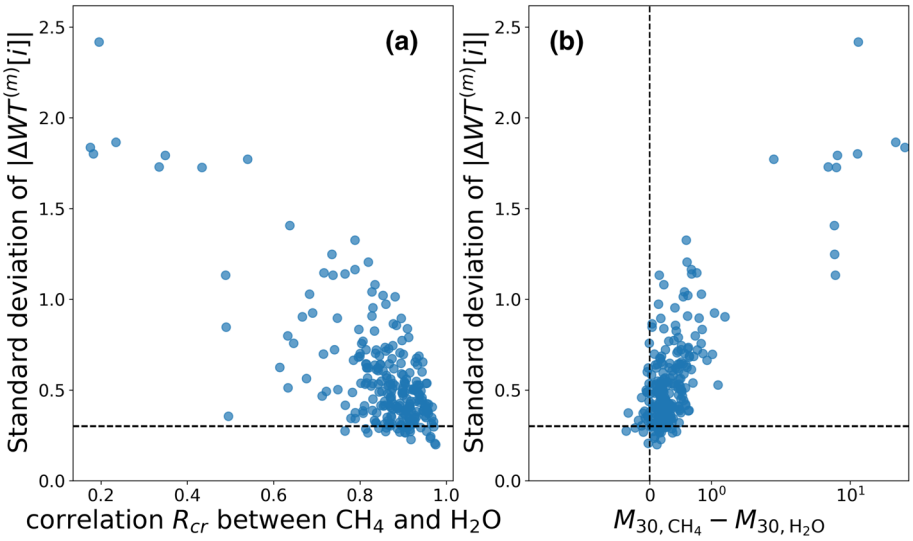

Fig. 2 Standard deviation of the difference of wavelet coefficients (Σ_{cr}) between CH_4 and H_2O as a function of **a** the correlation R_{cr} between the two scalars, and **b** the difference in skewness M_{30} between CH_4 and H_20 for each run included in the analysis. The threshold value $\Sigma_{cr} = 0.3$ is indicated by the dashed horizontal lines

The fraction A^+ of time in which attached eddies identify localized hotspots is then obtained by first back-transforming the filtered series of wavelet coefficients to the time domain, using only the non-zero coefficients for the hotspot and background series respectively as selected by the indicators $\delta_x\,(i, m)$ and $\delta_s\,(m)$

$$c_x\,(t) = \sum_{m=1}^{M} \sum_{i=1}^{2^{M-m}} \psi_{i,m}\,(i)\; WT_c^{(m)}\,[i]\,\delta_s\,(m)\,\delta_x\,(i, m)\,. \tag{9}$$

After partitioning the signal in the wavelet domain, in a second step CH_4 hotspots are individuated in the time domain by imposing the condition that the local power of the partitioned hotspot wavelet coefficients is sufficiently larger than the background variance. The fraction of time in which hotspots are active is obtained by the condition that $(c_h - median\,(c_h))^2 > \overline{c_b^2}$, i.e., whenever the squared fluctuations from the median of the hotspot concentration component (c_h) are larger than the variance of the background time series c_b. Note that with this definition we are separating intervals in which only a background flux occurs from intervals (labelled hotspot) in which the hotspot component is predominant. The fraction of time in which this occurs is denoted A^+, corresponding to the fraction of source area where integral-scale eddies carry the signature of hotspots at any given instant in time on average. Conversely, when this condition is not met (fraction $1 - A^+$ of the source area) only a background flux occurs. Based on this partition of the original time series, we compute the hotspot ($x = h$) and background ($x = b$) contributions to the overall scalar variance and flux. The fractions of total flux and total variance of each component are

$$f_x = \frac{1}{\overline{w'c'}} \frac{1}{N} \sum_{i=1}^{N} c_x'(i) w'(i) \delta_{t,x}(i) \tag{10}$$

and

$$v_x^+ = \frac{1}{\sigma_c^2}\frac{1}{N}\sum_{i=1}^{N} c_x'(i)^2 \delta_{t,x}(i), \tag{11}$$

where $\delta_{t,x}(i) = 1$ if the ith observation has been classified as hotspot ($x = h$) or background ($x = b$), and $\delta_{t,x}(i) = 0$ otherwise. As anticipated, the active fractional area of the footprint is

$$A^+ = \frac{1}{N}\sum_{i=1}^{N} \delta_{t,h}(i). \tag{12}$$

To test this partition methodology, the moments of the joint distribution of the scalar and vertical velocity fluctuations are computed. This is done both for the original time series and separately for the run intervals labelled as CH_4 background and hotspots respectively. Previous studies have shown that 4th order cumulant expansions suffice to explain the joint PDFs of CH_4 and w (Katul et al. 2018b). Therefore, the focus is on moments M_{ij} up to the 4th order. To characterize the statistical properties of the hotspot or background components of any scalar concentration, a partial mixed moments can be defined (for either $x = h, b$) as

$$M_{ij}^x = \frac{1}{\sigma_c^i \sigma_w^j}\frac{1}{N}\sum_{k=1}^{N} \left(c'(k)\right)^i \left(w'(k)\right)^j \delta_{t,x}(k). \tag{13}$$

While the partition method only uses values of the scalar wavelet coefficients, this test includes the interaction of the scalar with the vertical velocity fluctuations. Overall, this check shows that the background component moments are closer to the 1:1 line compared to the original time CH_4 series, and in particular the imbalance in the scalar skewness M_{30} appears reduced (Fig. 3). Note that in Fig. 3 the CH_4 background component is compared to H_2O moments computed by conditioning on the same background-only times, following Eq. 13. This conditioning is necessary to compare moments for the two concentration time series conditional to the same vertical velocity values.

An additional check can be performed by considering the transport efficiency e_T, which quantifies the ratio between direct and indirect flux as evaluated through quadrant analysis. Here, e_T is evaluated in the time domain for hotspot and background CH_4 components as $e_T = 1 - |\overline{F}_{ind}/\overline{F}_{dir}|$ where $\overline{F}_{ind}$ and $\overline{F}_{dir}$ are the covariances evaluated by including in the sum only indirect (in the case of CH_4, downward, i.e., inner and outer interactions only) or direct (upward, i.e., sweeps and ejections only) contributions to the flux respectively (Katul et al. 2018b). As done in the case of the mixed moments, we compare e_T for the CH_4 background component with its H_2O counterpart evaluated over the same time intervals. The CH_4 fluxes are characterized by a larger e_T when compared to other scalars (Fig. 4a), and this behaviour may be connected to the signature of localized hotspots leading to an alignment between large w' and c'.

In the case of CO_2, e_T appears lower than its H_2O counterpart. Again, this behaviour may be the direct effect of the inhomogeneity of the spatial distribution of CO_2 sources and sinks at the ground. The relatively inefficient CO_2 flux could originate from areas characterized by less dense vegetation, or from the interplay of photosynthethic activity (net sink) with the emission of bubbles also containing CO_2 from the peat, which would produce localized contributions of the opposite sign. As shown in Fig. 4a, e_T exhibits a clear dependence on the atmospheric stability as quantified by the MOST stability parameter (ζ). Overall, e_T tends to be larger for CH_4 when compared to H_2O regardless of ζ.

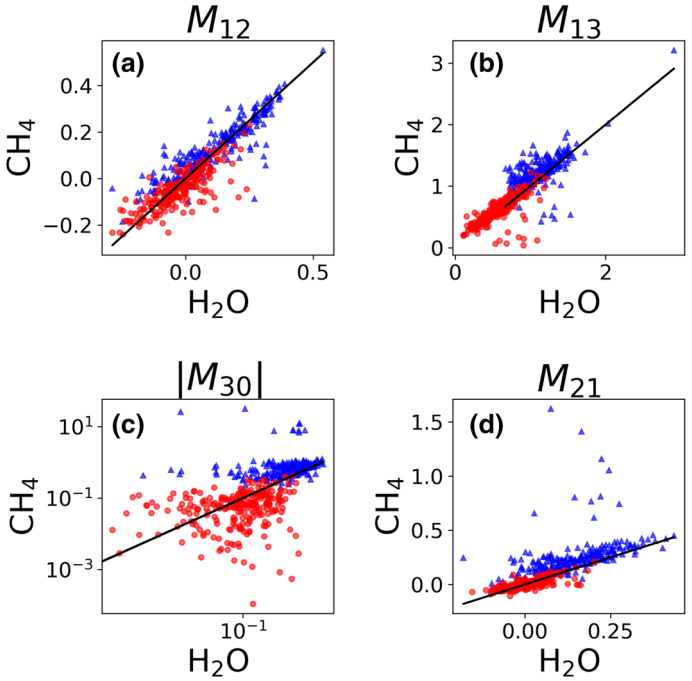

Fig. 3 Comparison of moments of the joint distribution of scalar quantities and vertical velocity, for both the original CH_4 and H_2O time series (blue data points) and the corresponding background-only values (red data points) for each run included in the analysis. The 1:1 relation is indicated by the black lines

However, when separately examining background and hotspot components, e_T appears lower for the former, and more in line with the corresponding e_T values observed for H_2O, as shown in Fig. 4b. Even though the partition methodology used here only employs information on the scalar concentrations, its results appear consistent even when considering the interaction with the vertical velocity fluctuations, and in particular the scalar transport efficiency e_T. Based on these observations, an extension of surface renewal theory is now introduced for characterizing the intermittent nature of CH_4 fluxes. The extension is based on the quantities v_x, f_x, and A^+ obtained through the wavelet partition performed here.

5 A Surface Renewal Approach for Continuous and Intermittent Scalar Sources

The classical surface renewal approach assumes a homogeneous scalar source at the ground, as may be the case for H_2O (at least when compared to the remaining scalars). The turbulent transport can be adequately described by an surface renewal scheme in which turbulent eddies are continuously touching the ground and are randomly renewed so that the distribution of residence times in contact with the ground is exponential (Danckwerts 1951). In conventional surface renewal theories, the mean residence time is of the order of the Kolmogorov time scale so that $b = \tau_\eta = (\nu/\epsilon)^{1/2}$ where ν is the kinematic viscosity of air and ϵ is the mean turbulence kinetic energy (TKE) dissipation rate. For a stationary, planar-homogeneous flow in the absence of subsidence and upon neglecting turbulent transport and pressure redistribution terms (Katul et al. 2011), the TKE budget is given as

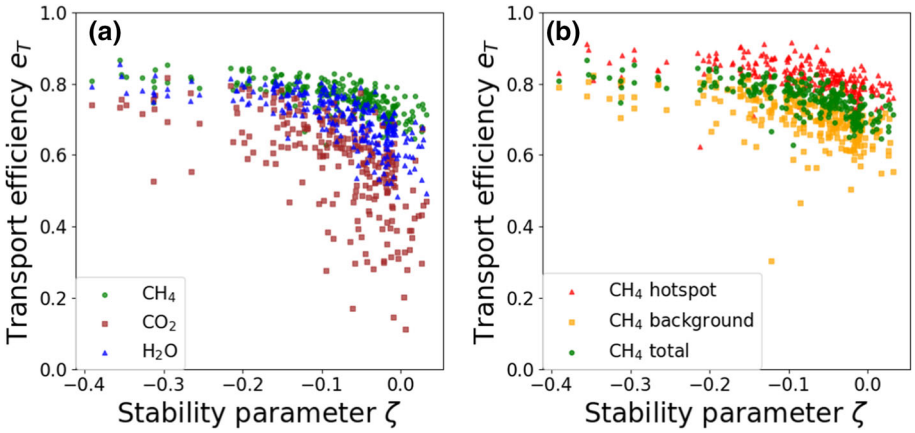

Fig. 4 **a** Dependence of scalar transport efficiencies e_T on the atmospheric stability parameter ζ for H_2O, CH_4. **b** The same quantity compute for CH_4 and for its hotspot and background components

$$\epsilon \simeq \frac{u_*^3}{k_v z}\phi_m(\zeta) + \frac{g}{T_a}\overline{w'T'}, \tag{14}$$

with k_v the von Kármán constant, ϕ_m the MOST correction function that varies with ζ (Foken and Nappo 2008; Stull 2012), $g = 9.8\,\mathrm{m\,s^{-2}}$ is the acceleration due to gravity and T_a the mean air temperature. The two terms on the right hand side of Eq. 14 correspond to mechanical production and buoyancy production (or destruction, depending on the sign of the Obukhov length L_{mo}) of TKE. Atmospheric surface layer flows over peatlands are characterized by high $Re_* = z_r u_*/\nu$ and a dynamically rough surface (i.e., z_0 is independent of Re_*). Therefore, ϵ was computed by evaluating the balance in Eq. 14 at a distance from the ground $h = 7.5 z_0$ (Brutsaert 2013), with z_0 computed from the mean velocity profile as $z_0 = z_r e^{-k_v U/u_*}$, where U is the mean longitudinal velocity measured at a distance z_r from the ground ($z_r = 2.8$ m in the experimental set-up here). The flux terms u_* and $\overline{w'T'}$ are evaluated at $z = z_r$ and are assumed constant with height. The sign of the flux is not predicted by the surface renewal model. Therefore, the skewness of the flux time series, its time directionality properties (Zorzetto et al. 2018), or simply the sign of the eddy-correlation flux (when this information is available) can be used.

Here, the analysis is restricted to the case of positive (i.e., upward) fluxes (H_2O and CH_4). When comparing results with $c = T$ or $c = CO_2$ time series, the sign of $\overline{w'c'}$ will be used. In field studies of methane, the source strength at the ground Δc is not usually known. Here, we estimate Δc as a function of the energy and skewness of the scalar fluctuations as $\Delta c = k_{sr}\sigma_c^{(I)} a_{sr,c} = k_{sr}\sigma_c^{(I)}\left(1 + |M_{30,c}|^{1/3}\right)$, where $M_{30,c}$ is the skewness of the scalar time series, and $\sigma_c^{(I)}$ the square root of the spectral energy density of the scalar c integrated over a range of scales around the integral time scale T_w (here set to the range of scales between 0.5 T_w and 5 T_w due to the limited frequency localization of the Haar decomposition). We found by comparison with eddy-covariance fluxes that the proportionality constant $k_{sr} \approx 4$ and this value applies for all scalar quantities examined. Based on previous results obtained for temperature, the quantity $k_{sr}\sigma_c^{(I)}$ may be interpreted as a difference between the maximum and minimum concentration fluctuations expected in a run (Frisch and Businger 1973; Katul et al. 1996), as driven by the difference between the source at the ground and background concentrations. Since the scalar variance varies with u_*, the correction factor $a_{sr,c}$ accounts

Table 1 Values used for the molecular diffusivity D_m and Schmidt number $Sc = \nu/D_m$ for the scalar quantities of interest

Quantity	$D_m(10^{-4}\ \ \mathrm{m^2 s^{-1}})$	$Sc\ \ (-)$
u	0.151	–
T	0.212	0.71
H_2O	0.24	0.59
CO_2	0.157	0.96
CH_4	0.222	0.68

for the possible asymmetry in the scalar time series, which is a statistical quantity expected to retain information on the injection of scalar variance in a turbulent flow (Warhaft 2000; Zorzetto et al. 2018). With these assumptions, the following expression for scalar fluxes can be derived, as done in Eq. 3

$$v_g = \frac{\overline{w'c'}}{\Delta c} = \frac{\overline{w'c'}}{k_{sr}\sigma_c^{(I)} a_{sr,c}} = \sqrt{\frac{D_m}{\tau_\eta}} = Sc^{-1/2}(\nu\epsilon)^{1/4}, \tag{15}$$

where v_g is a gas transfer velocity and $Sc = \nu/D_m$ is the molecular Schmidt number. The v_g emerging from this analysis is, as expected, consistent with the micro-eddy model given by $v_g \propto [Sc^{-1/2}(\nu\epsilon)^{1/4}]$ (Katul et al. 2018a), where $(\nu\epsilon)^{1/4}$ is the Kolmogorov velocity scale. The $v_g \sim Sc^{-1/2}$ has received wide support from experiments and direct numerical simulations in the limit of high Sc (Takagaki et al. 2016). The D_m used here for different scalar quantities are reported in Table 1 for convenience. Unlike water, diffusion of scalars in the atmosphere leads to an Sc close to unity and is suggestive that Sc adjustments to v_g are not as crucial for the scalars of interest here.

The surface renewal scheme proposed was then applied to different scalars (methane, water vapour, temperature) and to the longitudinal component of the velocity vector to further test the robustness of the approach, using the values of Sc given in Table 1 and ϵ estimated from Eq. 14. Figure 5 shows a comparison of this surface renewal scheme with eddy-covariance flux estimates for all 4 quantities. The method, after calibration of a single constant k_{sr} (which is the same for each scalar and constant across all runs) appears to reasonably reproduce all scalars, and surprisingly momentum fluxes (as noted in prior studies by Hanratty (1956)). Note however that the surface renewal is not fully prognostic when applied to momentum, since u_* is needed in the TKE budget to evaluate the Kolmogorov time scale. For CH_4 surface renewal and eddy-covariance flux estimates exhibit a larger scatter, and the presence of some very large outliers hints at the possible differences in ground sources when compared to the other scalars, which will be examined next.

5.1 Extension to Intermittent Surface Renewals

Since the complete surface renewal theory requires the description of small-scale quantities at the Kolmorogov scale and their spatial distribution, it is not feasible to reconstruct them using conventional eddy-covariance measurements. The current eddy-covariance measurements simply do not resolve such fine scales due to instrument separation and volume-averaging. To progress on an surface renewal theory that is mindful of such instrument limitations, a simplified intermittent model that will be based on surface renewal micro-eddy model (i.e., the bottleneck in the transport is dominated by Kolmogorov-scale eddies in the vicinity of the surface) while the intermittency of the process is described at the integral scale – i.e.,

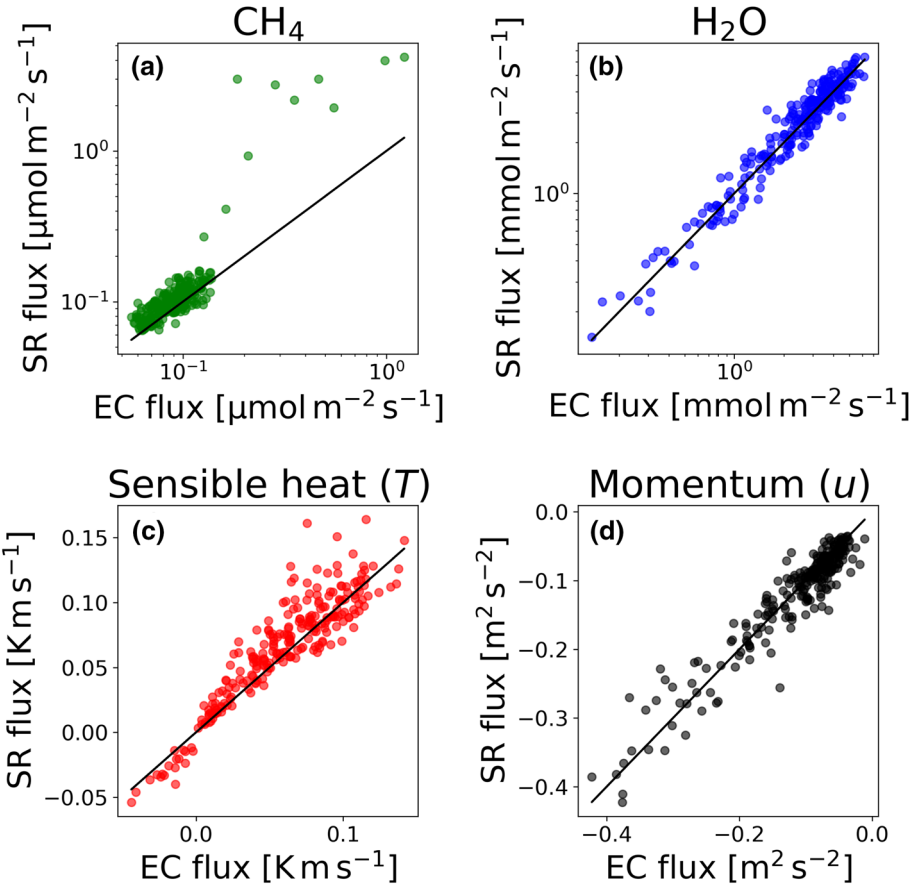

Fig. 5 Comparison between eddy-covariance (EC) and surface renewal (SR) fluxes for methane, sensible and latent heat fluxes, and (kinematic) momentum flux. Note that a logarithmic scale is used in panels **a** and **b**. In all panels, the 1 : 1 line is reported as reference

at the scales of eddies touching the ground, which may carry, or not, the signature of one or more CH_4 hotspots events. Therefore, the integral time scale of the measurements is associated with the smallest scale at which hotspot events can be detected, which therefore scales with the measurement height z_r. Given this separation of scales relevant for the overall scalar fluxes, the large-scale depiction of the intermittent source does not directly impact the shape of the distribution of eddy ages at the ground, and thus the scaling of the fluxes with Re_*. As is the case for the surface renewal micro-eddy model, both hotspot and background diffusive fluxes should scale as $Sc^{-1/2}Re_*^{-1/4}$. However, since the relative contributions of the two mechanisms is expected to change with environmental conditions, the overall flux may diverge from the $Re_*^{-1/4}$ scaling as anticipated from the larger scatter for CH_4 flux estimates when compared to other scalars (Fig. 5).

In this formulation, the overall flux is given by $\overline{F} = (1-A^+)\overline{F_b}+(A^+)\overline{F_h}$ i.e., is a weighted average of an hotspot flux $\overline{F_h}$ and a background flux $\overline{F_b}$, each weighted by the respective fractional contributing area of the footprint. Each of these two components has expression of the type derived in Eq. 15, but the two mass transfers are driven by different source

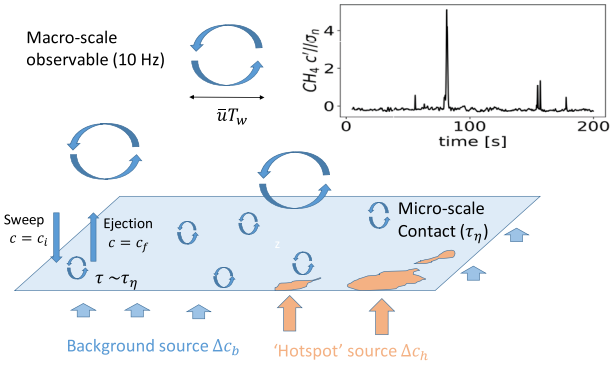

Fig. 6 Scheme of the transport mechanism for CH_4 near the surface. The figure represents an idealized patchy CH_4 source at the ground, emphasizing the small scale η of eddies dominating the interfacial gas transfer, and the integral scale $u \cdot T_w$ of the vertical velocity representing the large scales resolved by the tower measurements, which carry the integrated signature of the patchy CH_4 source at the ground

strengths denoted as Δc_b or Δc_h for the background and hotspot components respectively. Since the source strength is proportional to the square root of the scalar energy (over a given range of scales around T_w), we have that $\Delta c_b = k_{sr} a_{sr,b} \sigma_b^{(I)} / \sqrt{1 - A^+}$ and $\Delta c_h = k_{sr} a_{sr,h} \sigma_h^{(I)} / \sqrt{A^+}$, taking $\sigma_b^{(I)} = v_b^+ \cdot \sigma_c^{(I)}$ and $\sigma_h^{(I)} = v_h^+ \cdot \sigma_c^{(I)}$. Analogous to $a_{sr,c}$, the quantities $a_{sr,h}$ and $a_{sr,b}$ are evaluated for the two components using the skewness of the hotspot and background components alone as obtained following the wavelet partitioning scheme discussed in Sect. 4. Here, k_{sr} has the same value determined for the non-intermittent surface renewal approach, and again assumes a constant value across different runs and different scalars. Therefore, the overall flux can be expressed as

$$\overline{F} = \left(\sqrt{1 - A^+} + \sqrt{A^+} \frac{v_h^+}{v_b^+} \frac{a_{sr,h}}{a_{sr,b}} \right) k_{sr} v_b^+ a_{sr,b} \sigma_c^{(I)} \sqrt{\frac{D_m}{\tau_\eta}}, \tag{16}$$

where A^+ is the average fractional area characterized by integral-scale eddies carrying the signature of CH_4 hotspots. These quantities (A^+, Δc_h, and Δc_b) are all large-scale quantities and do not correspond to the Kolmogorov-scale quantities governing the mass exchange at the interface, but rather are linked to their integral-scale effect as captured by the scalar concentration measurement time series. For a schematic representation of the ISR scheme featuring the range of scales involved, see Fig. 6.

Scalar fluxes over a rough surface for near neutral atmospheric conditions as described by a micro-eddy type model (Brutsaert 1975) can be expressed in term of a dimensionless Dalton number $Da = F/(u_* \Delta c)$ as $Da = Sc^{-1/2} Re_*^{-1/4}$. Similarly, a dimensionless expression for the ISR fluxes can be derived here as

$$Da_b = \left(\sqrt{1 - A^+} + \sqrt{A^+} E^+ \right) Sc^{-1/2} Re_*^{-1/4}, \tag{17}$$

where two additional dimensionless numbers are now required describing the interplay of diffusive and hotspot contributions to the overall CH_4 fluxes. Again, the number A^+ represents the average fraction of area (or time) characterized by hotspot source (at the integral time scale); $E^+ = (a_{sr,h} v_h^+)/(v_b^+ a_{sr,b})$ represents the relative strength of hotspot sources at the ground with respect to the concentration gradient driving the diffusion process, and $Da_b = F/(u_* \Delta c_b)$.

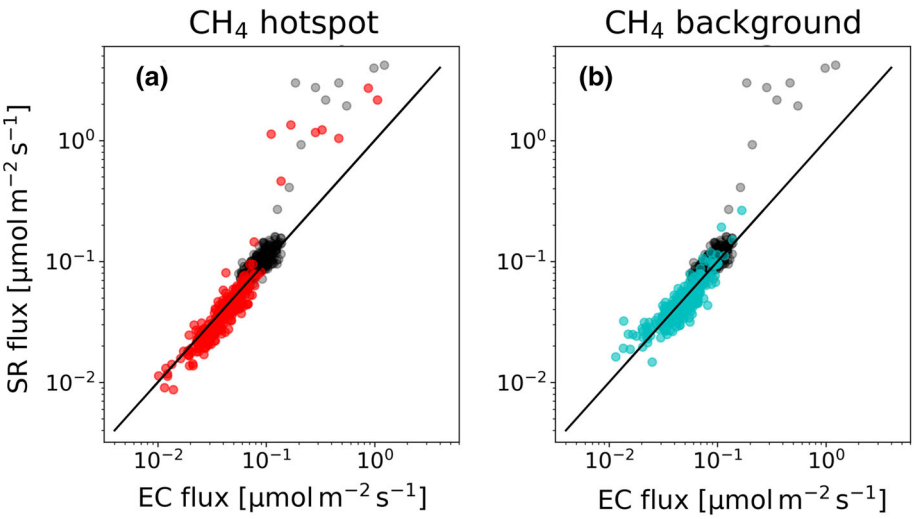

Fig. 7 Surface renewal estimates for the hotspot (red, panel a) and background (cyan, panel b) components of CH_4 compared with the overall CH_4 flux (black circles in the background). Surface renewal (SR) fluxes are compared with the corresponding wavelet—eddy-covariance fluxes (EC) partitioned through the wavelet scheme described in Sect. 4. The 1 : 1 line is reported as reference

The results of the CH_4 flux wavelet partition and its comparison with the (intermittent) surface renewal fluxes are reported in Fig. 7. The overall CH_4 fluxes exhibit a larger scatter when compared with H_2O, suggesting that the transport efficiency is more variable as determined by the interplay of hotspot and background fluxes. Comparing the hotspot and background components to the fluxes with their counterpart obtained through the wavelet partition scheme described in Sect. 4, again we can see that a micro-model type surface renewal scheme is appropriate for each component separately even though a larger scatter is present for the hotspot flux, which is responsible for the run-to-run variability observed for the overall CH_4 flux. In particular, the largest outliers observed for the overall flux are predominantly characterized by hotspot-type fluxes, as captured both by the wavelet partition scheme and the ISR-estimated flux.

6 Discussion

6.1 Transport Efficiency and Interpretation of Intermittent Surface Renewals Parameters

The gas transfer velocity and transport efficiency of the different gas transfer mechanisms are now considered. Generally, transport efficiency can be computed from eddy-covariance flux estimates as $\overline{w'c'}/\sigma_c/\sigma_w$ and is related to the asymmetry in the c', w' components by quadrant analysis (through the quantity e_T analyzed in Sect. 4), or through the slope β in the relaxed eddy accumulation method (Businger and Oncley 1990; Baker et al. 1992; Pattey et al. 1993). Transport efficiencies and gas transfer velocities ($\overline{w'c'}/\sigma_c$) are reported in Fig. 8, panels (a) and (b) respectively. Based on the wavelet partition scheme, the gas transfer velocities for hotspot and background CH_4 components can be computed as $(A^+\overline{F}_h)/(\sqrt{v_h^+/A^+}\sigma_c)$ and

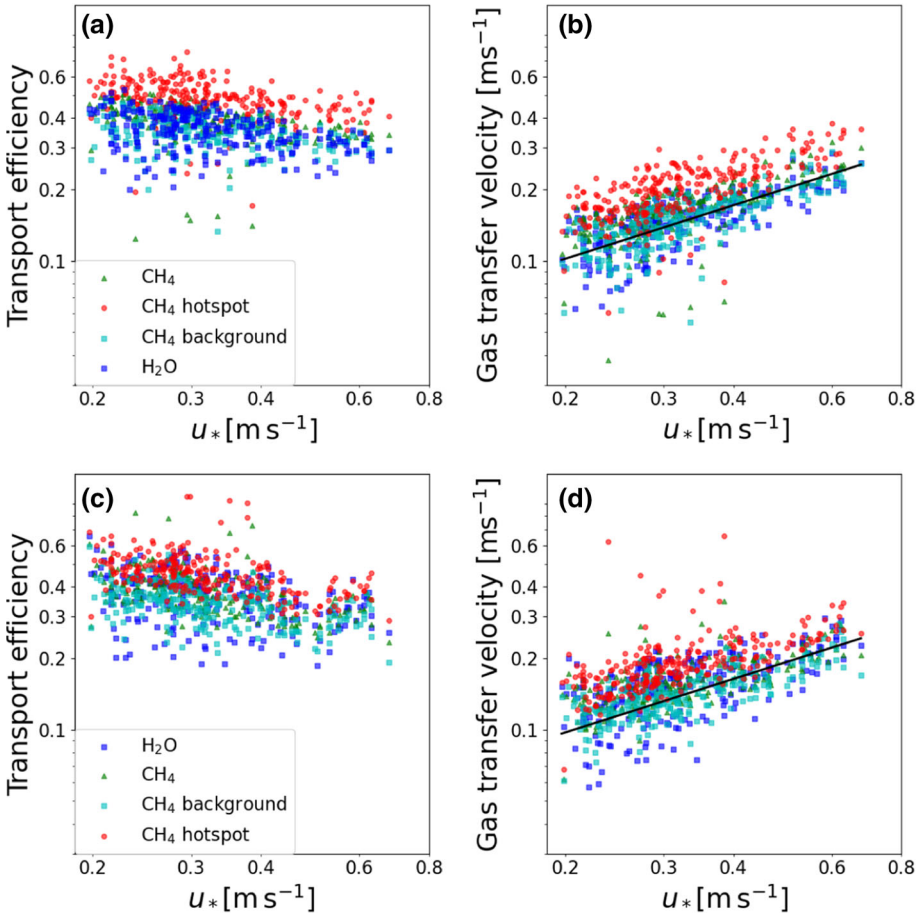

Fig. 8 Upper panels: eddy-covariance-estimated transport efficiency (**a**) and gas transfer velocity (**b**) for H_2O (blue), CH_4 (green) and its hotspot (red) and background (cyan) flux components as a function of u_*, obtained through the wavelet partition of the total CH_4 flux. For each component, each data point corresponds to a different 30-min run in our dataset. Lower Panels: surface-renewal-estimated transport efficiency (**c**) and gas transfer velocity (**d**) for H_2O (blue), CH_4 (green) and its hotspot H (red) and background B (cyan) flux components as a function of u_*. For each component, each data point corresponds to a different 30-min run in our dataset. The black lines show the 3/4 slope expected from the surface renewal scaling

$((1-A^+)\overline{F}_b)/(\sqrt{v_b^+/(1-A^+)}\sigma_c)$ respectively, where v_b^+ and v_h^+ are the dimensionless fractions of background and hotspot concentration standard deviation, respectively. From this analysis, the hotspot component tends to have a larger transport efficiency compared to the background, as foreshadowed by the difference between H_2O and CH_4 in the moments of the joint p.d.f. of (c' and w'). However, the overall dependence on u_* appears consistent between hotspot and background components, thus supporting the structure of the surface renewal model used here, where both components of the flux are assumed to scale with $u_*^{3/4}$. As shown in Fig. 8b, for both components the gas transfer velocity exhibits the same dependence on u_*.

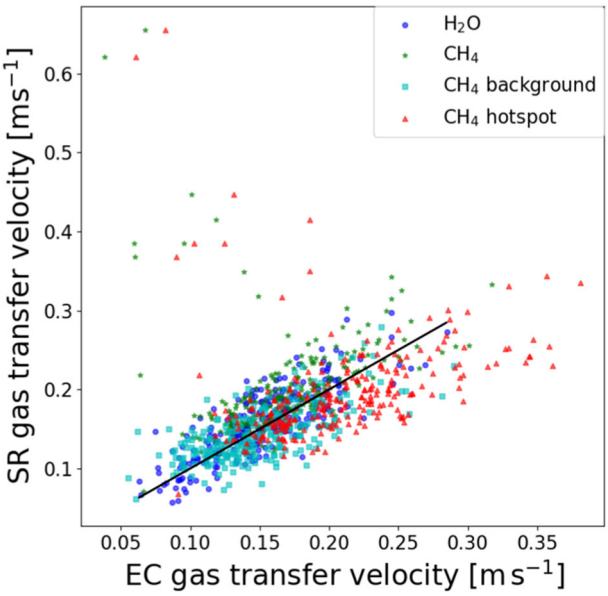

Fig. 9 Comparison of gas transfer velocities computed with the eddy-covariance (EC) and surface renewal (SR) approaches for H_2O (blue), CH_4 (green) and its hotspot (red) and background (cyan) flux components. The 1 : 1 line is reported as reference

A similar result is obtained from the analysis of surface renewal fluxes (Fig. 8, panels c and d). In this case, the gas transfer velocity is estimated dividing the surface renewal flux by the standard deviation of the scalar. Surface renewal estimates appear to satisfactorily reproduce CH_4 gas transfer velocities and, as in the case of eddy covariance, assigns a larger transport efficiency to the CH_4 intermittent component. Note that a discrepancy exists for the runs characterized by a very intense intermittent flux, for which surface renewal predicts a larger gas transfer velocity when compared to eddy-covariance estimates. This can also be seen by directly comparing surface renewal and eddy-covariance gas transfer velocity values as reported in Fig. 9, and is an effect of the large values of scalar skewness characterizing the runs with intense CH_4 hotspot events.

6.2 Effects of Intermittent Sources on CH_4 and CO_2 Scalar Concentrations

To elaborate on the effects of the intermittent CH_4 fluxes, and the results of the wavelet partition procedure, we focus our attention on a single run. We choose one of the most extreme runs in the dataset, recorded on 9 July 2013 at 1330 LT (local time = UTC + 3h), which is a day characterized by an exceptionally intense CH_4 flux, and for which the partition scheme identifies multiple source hotspots. For this run, the CH_4 time series is particularly asymmetric with several extreme values of the order of 10 standard deviations (Fig. 10) while the water vapour series exhibits ordinary statistical properties. As a consequence, the wavelet partition clearly classifies most of these large events as intermittent (Fig. 10c). Given the intensity of these concentration fluctuations, particular attention should be used when despiking the raw observations. However, we note that even the most intense CH_4

fluctuations observed in this run exhibit temporal coherence and were not removed by our preprocessing (Brock 1986).

Interestingly, CO_2 concentrations exhibit some positive concentration fluctuations that appear synchronous with their CH_4 counterparts. However, these CO_2 events are much less energetic when normalized by the variance of their respective series. This finding is consistent with the presence of localized ebullition events, with bubbles containing not only CH_4 but also CO_2. Gas chamber measurements indeed suggest that bubbles may be largely composed of methane, and partially filled with other gases such as N_2 or CO_2 (e.g., Männistö et al. 2019). If this is the case, the relative weakness of CO_2 bubble-related signal can be explained by considering the atmospheric mixing ratio of these two gases. The ratio between bubble CH_4 concentration (≈ 0.4, based on Männistö et al. 2019) and CH_4 concentration in air ($\approx 2 \times 10^{-6}$) is three orders of magnitude larger when compared to the ratio between bubble CO_2 (≈ 0.03, based on Männistö et al. 2019) and air CO_2 concentration ($\approx 4 \times 10^{-4}$). Hence, the occurrence of ebullition would determine spikes in CH_4 concentrations that are significantly more intense and easily detected compared to their CO_2 counterparts.

Moreover, these considerations may be used to explain the initial findings that CO_2 transport efficiency is lower than H_2O, a behaviour opposite to what was observed for CH_4 (Fig. 4a). In the case of CH_4, the occurrence of ebullition determines an increased transport efficiency with the most intense build-up in methane concentration being transported in few intense ejection events. These events significantly add to the already positive background diffusive flux. However, during daytime (which is the case for most of the runs analyzed here) the overall CO_2 flux is downward due to photosynthetic activity. However, the sporadic release of CO_2-containing bubbles determines an inflated fraction of positive CO_2 ejection and thus an overall reduced e_T for the total downward flux.

The effect of intermittent scalar sources on transport efficiency can also be appreciated in Fig. 11, where quadrant plots of vertical velocity w' and scalar concentration fluctuations c' are reported for the same run. For CH_4, and to a lesser extent for CO_2, high-magnitude scalar fluctuations preferably occur during ejection events. Note that for CO_2, for which $\overline{w'c'} < 0$, these events act against the average scalar gradient and therefore act to reduce the overall transport efficiency. The opposite is the case for CH_4, with an increased overall transport efficiency compared to that of the reference scalar (H_2O).

This behaviour can also be seen in Fig. 12, where the daily cycle of scalar fluxes is shown as estimated by either eddy-covariance or non-intermittent surface renewal theory. Methane fluxes do not show any clear diurnal variability and are dominated by the few already noted highly intermittent runs. On the other hand, H_2O, CO_2 and sensible heat fluxes exhibit diurnal variability as expected. However, it is interesting to note that if one focuses on surface renewal estimates and on the few runs supposedly characterized by intense ebullition, a large discrepancy can be observed between eddy-covariance and surface renewal fluxes for CO_2. This finding again supports the picture regarding intermittent CO_2 flux, which again would require an ISR model to be described as done for CH_4. In particular, it is the skewness term used in approximating Δc that produces this behavior. This behaviour thus suggests the possibility to observe runs in which the ground is overall a CO_2 sink but the CO_2 skewness is positive due to the effect of localized ejections.

An ISR scheme analogous to that developed for CH_4 here could describe this behaviour after partitioning the time series in its background (downward) and intermittent (with a possible upward) CO_2 flux components. The results of such an ISR model applied to CO_2 fluxes are shown in Fig. 13. The results are overall consistent with the eddy-covariance results, and the hotspot fraction of the flux is generally lower than in the case of CH_4. In some cases the sign of hotspots and backround fluxes differs. As already seen in Fig. 10,

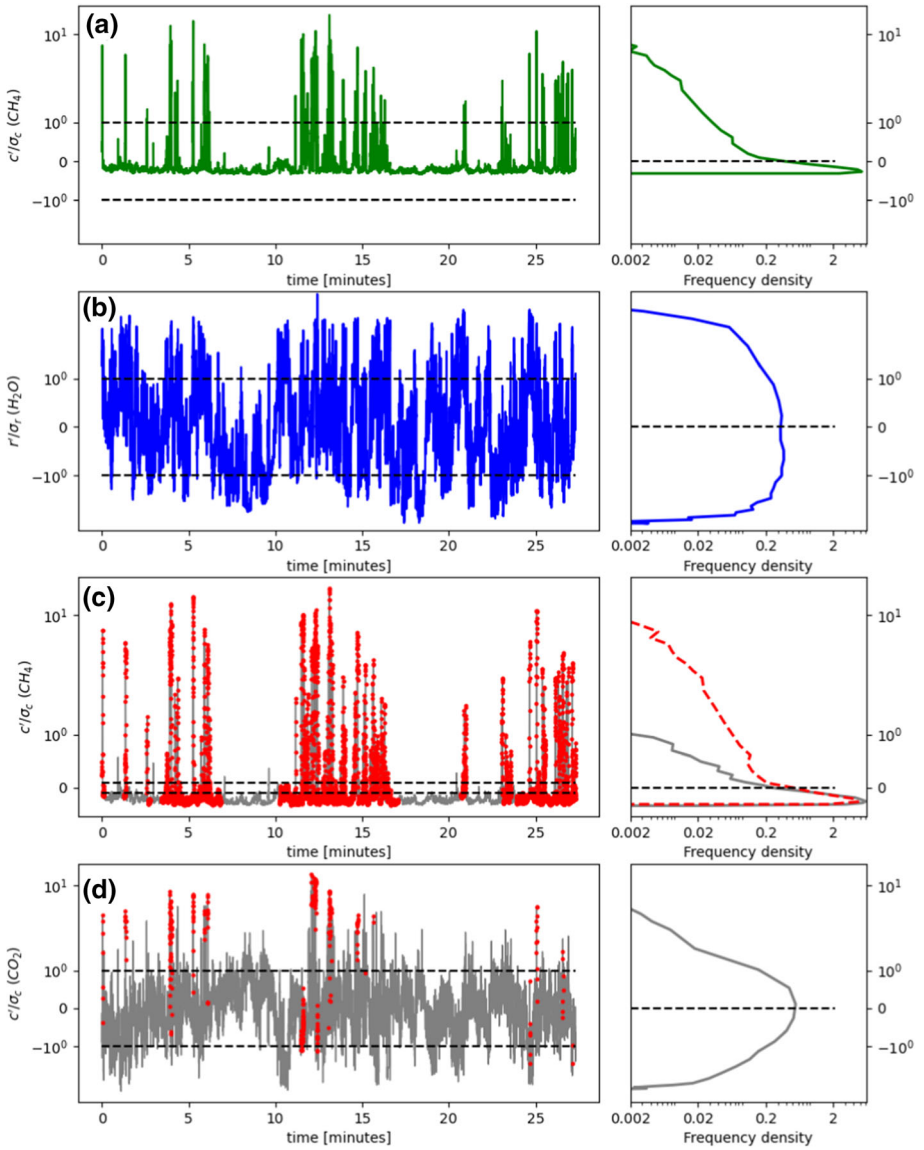

Fig. 10 Example of run made on 9 July 2013 1330 LT (local time = UTC + 3h), characterized by very intense CH_4 hotspots. The figure features **a** the normalized methane concentration (green), **b** water vapour (blue) and **c** the results of the partition (grey and red indicating original time series and hotspot components respectively). A comparison with the corresponding CO_2 time series is featured in the lower panel, where red circles denote points for which the corresponding CH_4 concentration exceeds $3\sigma_c$ (**d**). For each time series, the dashed horizontal lines show the 1 standard deviation bands around the mean (computed for the background component only in panel **c**). The pdfs of normalized scalar fluctuations are included for comparison. The pdfs corresponding to panel **c** include both that of hotspot only (red dashed line) and background only (grey line) components

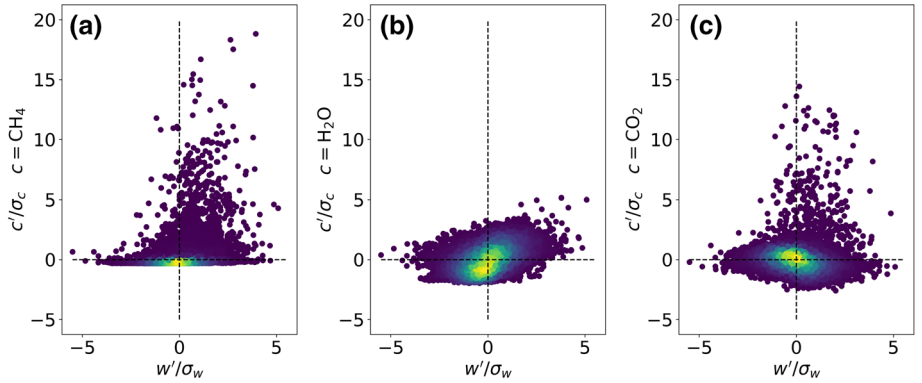

Fig. 11 For the same run shown in Fig. 10, quadrant plots of vertical velocity fluctuations w' and scalar concentration fluctuations c' for the three scalars $c = CH_4$ (panel **a**), H_2O (**b**), and CO_2 (**c**). The colour is proportional to the density of scatter points

some positive CO_2 spikes are coherent with their CH_4 counterparts. It is therefore possible that the interplay of these different CO_2 transport mechanisms (negative background flux and positive short-duration hotspot events) leads to the observed reduction in the overall transport efficiency for CO_2 when compared to the reference H_2O. These results however are not as clear as those obtained for CH_4, and may represent the combined effect of both release of bubbles and inhomogeneity in the CO_2 sinks at the surface (the vegetation is patchy).

6.3 Relation Between Partitioned CH_4 Fluxes and Environmental Parameters

How the parameters of the ISR scheme derived above describing CH_4 hotspots vary with differing environmental and flow conditions is now discussed. The seasonal variability of the methane fluxes is reported in Fig. 14a. Figure 14b shows the seasonal variability of the hotspot fractions of CH_4 flux (f_h), variance (v_h^+), and footprint area A^+. The clear outliers occurring around the day 9 July 2013 are characterized by intense CH_4 emissions, and by hotspots dominating the mass transfer mechanism. As an example, we have shown one of these runs in Fig. 10.

The relation between CH_4 fluxes and key environmental parameters is now considered. It is known that variability in water-table depth relative to the peatland surface and changes in atmospheric pressure impact CH_4 fluxes (Fig. 15). While overall there is no clear dependence on either, it is interesting to note that the runs characterized by very high CH_4 fluxes all occur for relatively high water-table levels and in decreasing atmospheric pressure conditions. This picture is consistent with the conditions for which CH_4 ebullition is expected to occur (Mattson and Likens 1990).

We can conjecture that for most of the runs, the mechanisms determining intermittent fluxes may be variable, and include non-homogeneous terrain, variable microbial activity, and some ebullition. However, in about 10 cases, the runs are characterized by unusually intense CH_4 positive fluctuations that give rise to fluxes an order of magnitude larger than median seasonal values. For these runs, the evidence analyzed here would suggest ebullition is the primary cause for these events. This appears to be the case because (i) they all occur for high water table levels, (ii) they all appear for decreasing atmospheric pressure values, and (iii) they are accompanied by a similar (albeit weaker) behaviour observed for the CO_2 time

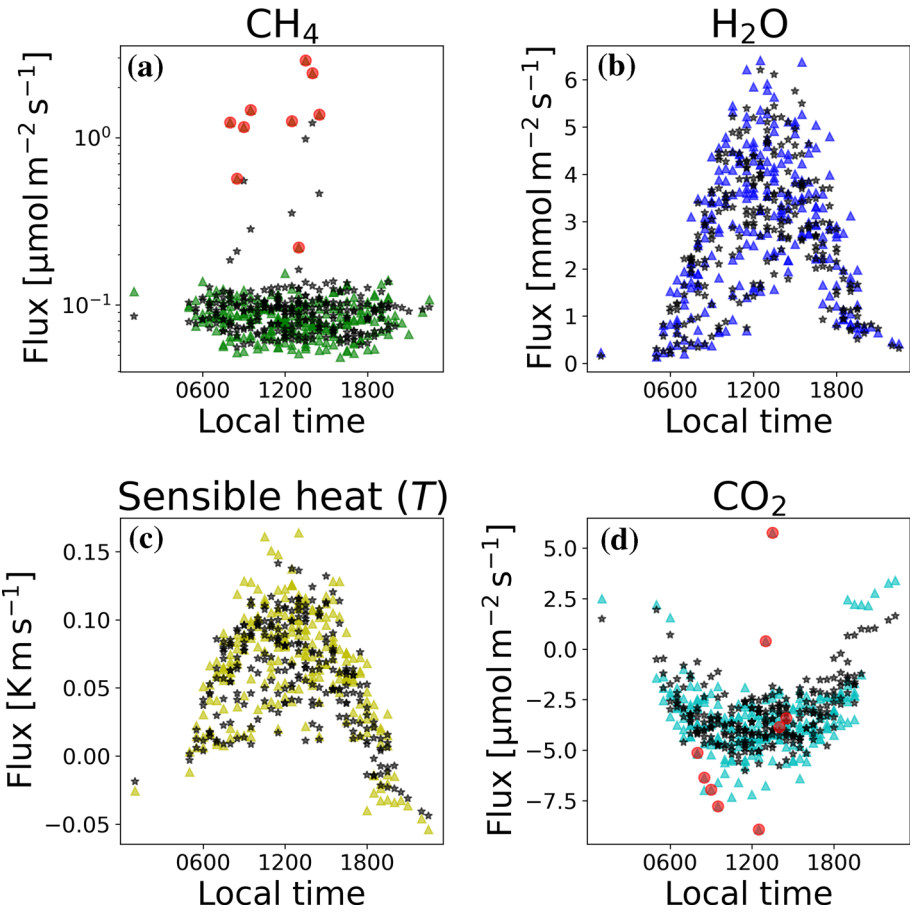

Fig. 12 Daily cycles of surface renewal (black stars) and eddy-covariance flux (colored triangles) estimates for various scalars, for all the runs in our dataset. Note the outliers for CH_4 and CO_2 corresponding to large fluctuations in the concentration time series (marked in red for surface renewal CH_4 fluxes larger than $0.004\ \text{mol m}^{-2}\ \text{s}^{-1}$)

series, which is consistent with a mixture of the two gases being released at the interface in the presence of bubbles.

7 Conclusions

An ISR scheme was proposed with the objective of characterizing the interplay and relative importance of diffusive and intermittent fluxes of methane over boreal peatlands. This model, while still describing the interfacial mass transport as a function of Schmidt number Sc and Reynolds number Re_*, depends on additional parameters related to the spatial intermittency of the fluxes (A^+) and the relative strength of intermittent and background (i.e., continuous) scalar sources at the interface (E^+). In the context of CH_4 emissions from boreal wetlands, the intermittent hotspots detected with this framework can be linked either to the occurrence of ebullition, or to the non-homogeneous distribution of plants and microbial activity. However,

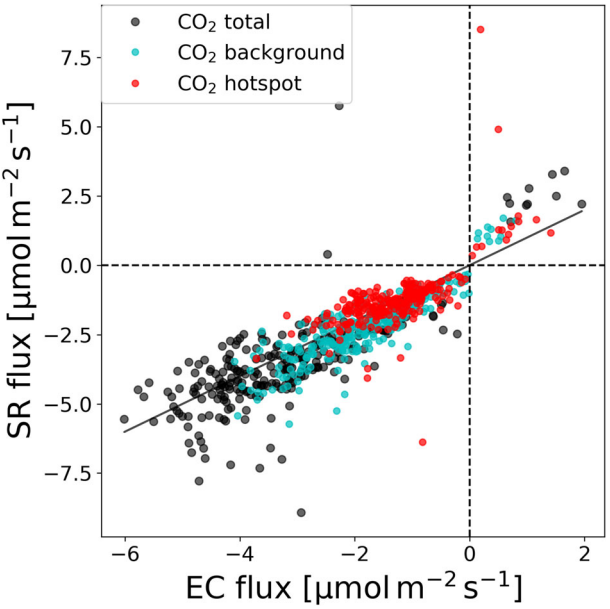

Fig. 13 Partition of the total CO_2 flux (black circles) in background B (cyan) and hotspot components H (red), comparing results obtained with the surface renewal (SR) and eddy covariance (EC) applied to the partitioned CO_2 time series. The black line indicates the 1:1 relation

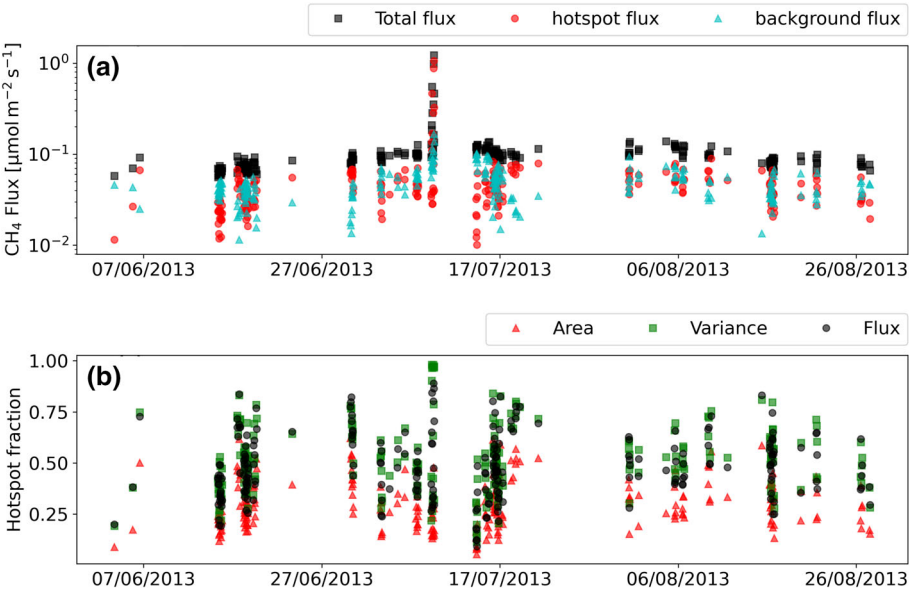

Fig. 14 Panel **a**: Seasonal variability of the total methane flux and of its hotspot and background components throughout the period of measurement analyzed. Panel **b**: Fraction of hotspot flux (black circle markers), scalar variance (green squares) and fractional footprint area (red triangles) during the same time interval

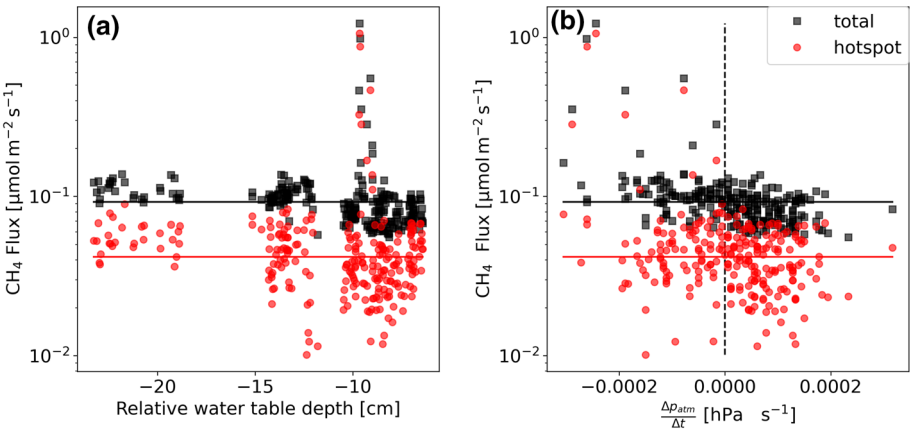

Fig. 15 Dependence of CH_4 flux on **a** water-table depth relative to the peatland surface, and **b** atmospheric pressure tendency (increment in atmospheric pressure computed for the 30-min period corresponding to each run). The horizontal lines show the average values for the two samples

the analysis of the CH_4 events characterized by the largest magnitudes, together with relevant environmental parameters, suggest that the sporadic release of bubbles may be at the origin of the most intense hotspot events.

Partitioning CH_4 fluxes with respect to a reference scalar (H_2O) suggested that spatial non-homogeneity of the CH_4 source, and in particular hotspots possibly related to ebullition, may be the primary cause for the observed statistical properties of CH_4 concentration traces: In particular, the skewed and non-Gaussian character of their PDFs, and the larger transport efficiency e_T compared to other scalars (e.g., temperature, water vapour). To the contrary, lower values of e_T are computed for CO_2 when compared to H_2O. This is expected and indirectly supports the conclusions for CH_4. In the case of CO_2, the presence of localized sources (possibly related to sporadic bubble release) lead to a decrease in the overall transport efficiency for the (downward) CO_2 flux.

These findings for CH_4 and CO_2 do not imply that the intermittency of the scalar source (i.e., the presence of hotspot events) must be in phase with sweeps and ejections. Rather, it appears that ejections are the most efficient mechanism acting to remove CH_4-enriched air parcels from the surface following a localized release of the gas.

The results here suggest that surface renewals, as well as the ISR extension for spatially inhomogeneous sources, can be complementary to eddy-covariance measurements in quantifying scalar fluxes, and instrumental in detecting contributions to CH_4 fluxes from intermittent sources. This information is practically relevant for the purpose of upscaling point measurements of CH_4 fluxes performed with the use of gas chambers. Given the limited time and spatial coverage of such field measurements, the information provided by methods such as ISR can be relevant for planning and interpreting the results obtained from field campaigns, now increasing in number and coverage for CH_4.

Acknowledgements EZ acknowledges support from the National Aeronautics and Space Administration (NASA NESSF Fellowship 80NSSC17K0364). GK was partially supported by the US National Science Foundation (NSF-AGS-1644382, NSF-IOS-1754893, NSF-AGS-2028633) and the University of Helsinki during a sabbatical leave from Duke University in 2017. The Python code used in this study is freely available at https://github.com/EnricoZorzetto/methane_isr under the MIT license.

References

Antonia R, Chambers A, Friehe C, Van Atta C (1979) Temperature ramps in the atmospheric surface layer. J Atmos Sci 36(1):99–108

Asher WE, Pankow JF (1991) Prediction of gas/water mass transport coefficients by a surface renewal model. Environ Sci Technol 25(7):1294–1300

Assouline S, Tyler SW, Tanny J, Cohen S, Bou-Zeid E, Parlange M, Katul GG (2008) Evaporation from three water bodies of different sizes and climates: measurements and scaling analysis. Adv Water Resour 31(1):160–172

Aulakh MS (2001) Methane emissions from rice fields-quantification, mechanisms, role of management, and mitigation options. Adv Agron 70:193–260

Baker J, Norman J, Bland W (1992) Field-scale application of flux measurement by conditional sampling. Agric For Meteorol 62(1–2):31–52

Baldocchi D, Detto M, Sonnentag O, Verfaillie J, Teh YA, Silver W, Kelly NM (2012) The challenges of measuring methane fluxes and concentrations over a peatland pasture. Agric For Meteorol 153:177–187

Bartlett KB, Harriss RC (1993) Review and assessment of methane emissions from wetlands. Chemosphere 26(1–4):261–320

Beetz S, Liebersbach H, Glatzel S, Jurasinski G, Buczko U, Höper H (2013) Effects of land use intensity on the full greenhouse gas balance in an Atlantic peat bog. Biogeosciences 10(2):1067–1082

Brock FV (1986) A nonlinear filter to remove impulse noise from meteorological data. J Atmos Ocean Tech 3(1):51–58

Brutsaert W (1965) A model for evaporation as a molecular diffusion process into a turbulent atmosphere. J Geophys Res 70(20):5017–5024

Brutsaert W (1975) A theory for local evaporation (or heat transfer) from rough and smooth surfaces at ground level. Water Res Res 11(4):543–550

Brutsaert W (2013) Evaporation into the atmosphere: theory, history and applications, vol 1. Springer, Berlin

Bubier J, Moore T, Roulet N (1993) Methane emissions from wetlands in the midboreal region of northern Ontario, Canada. Ecology 74(8):2240–2254

Bullin J, Dukler A (1972) Random eddy models for surface renewal: formulation as a stochastic process. Chem Eng Sci 27(2):439–442

Businger JA, Oncley SP (1990) Flux measurement with conditional sampling. J Atmos Ocean Tech 7(2):349–352

Byrne KA, Chojnicki B, Christensen TR, Drosler M, Frolking S, Lindroth A, Mailhammer J, Malmer N, Selin P, Turunen J et al (2004) Eu peatlands: current carbon stocks and trace gas fluxes. Geosphere-Biosphere Centre, University of Lund, Sweden, Tech Rep Report 4/2004 to Concerted action: synthesis of the European Greenhouse Gas Budget

Cava D, Katul G, Sempreviva AM, Giostra U, Scrimieri A (2008) On the anomalous behaviour of scalar flux-variance similarity functions within the canopy sub-layer of a dense alpine forest. Boundary-Layer Meteorol 128(1):33–57

Clayson C, Fairall C, Curry J (1996) Evaluation of turbulent fluxes at the ocean surface using surface renewal theory. J Geophys Res Oceans 101(C12):28503–28513

Danckwerts P (1951) Significance of liquid-film coefficients in gas absorption. Ind Eng Chem 43(6):1460–1467

Foken T (2006) 50 years of the Monin–Obukhov similarity theory. Boundary-Layer Meteorol 119(3):431–447

Foken T, Nappo CJ (2008) Micrometeorology, vol 2. Springer, Berlin

Foken T, Wichura B (1996) Tools for quality assessment of surface-based flux measurements. Agric For Meteorol 78(1–2):83–105

Fortescue G, Pearson J (1967) On gas absorption into a turbulent liquid. Chem Eng Sci 22(9):1163–1176

Frisch AS, Businger JA (1973) A study of convective elements in the atmospheric surface layer. Boundary-Layer Meteorol 3(3):301–328

Garbe CS, Jähne B, Haußecker H (2002) Measuring the sea surface heat flux and probability distribution of surface renewal events, American Geophysical Union (AGU), pp 109–114

Garbe CS, Schimpf U, Jähne B (2004) A surface renewal model to analyze infrared image sequences of the ocean surface for the study of air-sea heat and gas exchange. J Geophys Res Oceans 109(C8):1–18

Haghighi E, Or D (2013) Evaporation from porous surfaces into turbulent airflows: coupling eddy characteristics with pore scale vapor diffusion. Water Resour Res 49(12):8432–8442

Haghighi E, Or D (2015a) Linking evaporative fluxes from bare soil across surface viscous sublayer with the Monin–Obukhov atmospheric flux-profile estimates. J Hydrol 525:684–693

Haghighi E, Or D (2015b) Thermal signatures of turbulent airflows interacting with evaporating thin porous surfaces. Int J Heat Mass Transf 87:429–446

Hanratty TJ (1956) Turbulent exchange of mass and momentum with a boundary. AIChE J 2(3):359–362
Harriott P (1962) A random eddy modification of the penetration theory. Chem Eng Sci 17(3):149–154
Herbst M, Friborg T, Ringgaard R, Soegaard H (2011) Interpreting the variations in atmospheric methane fluxes observed above a restored wetland. Agric For Meteorol 151(7):841–853
Higbie R (1935) The rate of absorption of a pure gas into a still liquid during short periods of exposure. Trans AIChE 31:365–389
Hill RJ (1989) Implications of Monin–Obukhov similarity theory for scalar quantities. J Atmos Sci 46(14):2236–2244
Hommeltenberg J, Mauder M, Drösler M, Heidbach K, Werle P, Schmid HP (2014) Ecosystem scale methane fluxes in a natural temperate bog-pine forest in southern germany. Agric For Meteorol 198:273–284
Horvath IR, Chatterjee SG (2018) A surface renewal model for unsteady-state mass transfer using the generalized Danckwerts age distribution function. R Soc Open Sci 5(5):172423
Iwata H, Hirata R, Takahashi Y, Miyabara Y, Itoh M, Iizuka K (2018) Partitioning eddy-covariance methane fluxes from a shallow lake into diffusive and ebullitive fluxes. Boundary-Layer Meteorol 169(3):413–428
Katul G, Liu H (2017) A Kolmogorov–Brutsaert structure function model for evaporation into a turbulent atmosphere. Water Resour Res 53(5):3635–3644
Katul G, Hsieh CI, Oren R, Ellsworth D, Phillips N (1996) Latent and sensible heat flux predictions from a uniform pine forest using surface renewal and flux variance methods. Boundary-Layer Meteorol 80(3):249–282
Katul G, Mammarella I, Grönholm T, Vesala T (2018a) A structure function model recovers the many formulations for air-water gas transfer velocity. Water Resour Res 54(9):5905–5920
Katul G, Peltola O, Grönholm T, Launiainen S, Mammarella I, Vesala T (2018b) Ejective and sweeping motions above a peatland and their role in relaxed-eddy-accumulation measurements and turbulent transport modelling. Boundary-Layer Meteorol 169(2):163–184
Katul G, Li D, Manes C (2019) A primer on turbulence in hydrology and hydraulics: the power of dimensional analysis. Wiley Interdiscip Rev Water 6(2):e1336
Katul GG, Parlange MB, Chu CR (1994) Intermittency, local isotropy, and non-Gaussian statistics in atmospheric surface layer turbulence. Phys Fluids 6(7):2480–2492
Katul GG, Konings AG, Porporato A (2011) Mean velocity profile in a sheared and thermally stratified atmospheric boundary layer. Phys Rev lett 107(26):268502
Kermani A, Shen L (2009) Surface age of surface renewal in turbulent interfacial transport. Geophys Res Lett 36(10):1–5
Knox SH, Jackson RB, Poulter B, McNicol G, Fluet-Chouinard E, Zhang Z, Hugelius G, Bousquet P, Canadell JG, Saunois M et al (2019) Fluxnet-CH4 synthesis activity: objectives, observations, and future directions. Bull Am Meteorol Soc 100(12):2607–2632
Komori S, Nagaosa R, Murakami Y (1990) Mass transfer into a turbulent liquid across the zero-shear gas–liquid interface. AIChE J 36(6):957–960
Koppel L, Patel R, Holmes J (1966) Statistical models for surface renewal in heat and mass transfer: Part i. Dependence of average transport coefficients on age distribution. AIChE J 12(5):941–946
Kumar P, Foufoula-Georgiou E (1997) Wavelet analysis for geophysical applications. Rev Geophys 35(4):385–412
Lai D (2009) Methane dynamics in northern peatlands: a review. Pedosphere 19(4):409–421
Lamont JC, Scott D (1970) An eddy cell model of mass transfer into the surface of a turbulent liquid. AIChE J 16(4):513–519
Li D, Katul GG, Liu H (2018) Intrinsic constraints on asymmetric turbulent transport of scalars within the constant flux layer of the lower atmosphere. Geophys Res Lett 45(4):2022–2030
Mallat SG (1989) A theory for multiresolution signal decomposition: the wavelet representation. IEEE Trans Pattern Anal Mach Intell 11(7):674–693
Männistö E, Korrensalo A, Alekseychik P, Mammarella I, Peltola O, Vesala T, Tuittila ES (2019) Multi-year methane ebullition measurements from water and bare peat surfaces of a patterned boreal bog. Biogeosciences 16(11):2409–2421
Mattson MD, Likens GE (1990) Air pressure and methane fluxes. Nature 347(6295):718–719
Meneveau C (1991) Analysis of turbulence in the orthonormal wavelet representation. J Fluid Mech 232:469–520
Monin A, Obukhov A (1954) Dimensionless characteristics of turbulence in the surface layer. Akad Nauk SSSR Geofiz Inst Tr 24:163–187
Moore TR, De Young A, Bubier JL, Humphreys ER, Lafleur PM, Roulet NT (2011) A multi-year record of methane flux at the Mer Bleue bog, southern Canada. Ecosystems 14(4):646
Musschenga E, Hamersma P, Fortuin J (1992) Momentum, heat and mass transfer in turbulent pipe flow: the extended random surface renewal model. Chem Eng Sci 47(17–18):4373–4392

National Land Survey of Finland (2018) Topographic database. https://www.maanmittauslaitos.fi/en/opendata-licence-cc40
Pattey E, Desjardins R, Rochette P (1993) Accuracy of the relaxed eddy-accumulation technique, evaluated using co 2 flux measurements. Boundary-Layer Meteorol 66(4):341–355
Peltola O, Mammarella I, Haapanala S, Burba G, Vesala T (2013) Field intercomparison of four methane gas analyzers suitable for eddy covariance flux measurements. Biogeosciences 10(6):3749–3765
Peltola O, Hensen A, Helfter C, Belelli Marchesini L, Bosveld F, Van Den Bulk W, Elbers J, Haapanala S, Holst J, Laurila T et al (2014) Evaluating the performance of commonly used gas analysers for methane eddy covariance flux measurements: the InGOS inter-comparison field experiment. Biogeosci Discuss 11(1):797–852
Perlmutter D (1961) Surface-renewal models in mass transfer. Chem Eng Sci 16(3–4):287–296
Qiu J, Su HB, Watanabe T, Brunet Y et al (1995) Surface renewal analysis: a new method to obtain scalar fluxes. Agric For Meteorol 74(1–2):119–137
Rinne J, Riutta T, Pihlatie M, Aurela M, Haapanala S, Tuovinen JP, Tuittila ES, Vesala T (2007) Annual cycle of methane emission from a boreal fen measured by the eddy covariance technique. Tellus B Chem Phys Meteorol 59(3):449–457
Riutta T, Korrensalo A, Laine AM, Laine J, Tuittila ES (2020) Interacting effects of vegetation components and water level on methane dynamics in a boreal fen. Biogeosciences 17(3):727–740
Scanlon TM, Albertson JD (2001) Turbulent transport of carbon dioxide and water vapor within a vegetation canopy during unstable conditions: identification of episodes using wavelet analysis. J Geophys Res Atmos 106(D7):7251–7262
Schaller C, Göckede M, Foken T (2017) Flux calculation of short turbulent events-comparison of three methods. Atmos Meas Tech 10(3):869–880
Schaller C, Kittler F, Foken T, Göckede M (2019) Characterisation of short-term extreme methane fluxes related to non-turbulent mixing above an arctic permafrost ecosystem. Atmos Chem Phys 19(6):4041–4059
Seo YG, Lee WK (1988) Single-eddy model for random surface renewal. Chem Eng Sci 43(6):1395–1402
Spano D, Snyder R, Duce P et al (1997) Surface renewal analysis for sensible heat flux density using structure functions. Agric For Meteorol 86(3–4):259–271
Starkenburg D, Metzger S, Fochesatto GJ, Alfieri JG, Gens R, Prakash A, Cristóbal J (2016) Assessment of despiking methods for turbulence data in micrometeorology. J Atmos Ocean Tech 33(9):2001–2013
Stull RB (2012) An introduction to boundary layer meteorology, vol 13. Springer, Berlin
Takagaki N, Kurose R, Kimura A, Komori S (2016) Effect of Schmidt number on mass transfer across a sheared gas–liquid interface in a wind-driven turbulence. Sci Rep 6(37):059
Theofanous T, Houze R, Brumfield L (1976) Turbulent mass transfer at free, gas–liquid interfaces, with applications to open-channel, bubble and jet flows. Int J Heat Mass Transf 19(6):613–624
Thomson G, Silver R (1972) Reynolds flux and Danckwerts surface renewal theory. Int J Heat Mass Transf 15(6):1284–1287
Warhaft Z (2000) Passive scalars in turbulent flows. Ann Rev Fluid Mech 32(1):203–240
Wyngaard JC (2010) Turbulence in the atmosphere. Cambridge University Press, Cambridge
Zorzetto E, Bragg A, Katul G (2018) Extremes, intermittency, and time directionality of atmospheric turbulence at the crossover from production to inertial scales. Phys Rev Fluids 3(9):094604